Analysis of photographically measured crack development from shear tests on large bridge girders

Shaoyun Sun,
Daniel A. Kuchma,
and Kang Su Kim

Editor's quick points

- An experimental research program was conducted on the shear behavior of large bulb-tee girders that were simply supported and subjected to uniformly distributed loads.
- It was observed in this research that the angle of diagonal cracking could be predicted using Mohr's circle of stress.
- Based on test data, equations for computing the average spacing and maximum crack width of inclined cracks were proposed to overcome unconservative results obtained by current methods.

According to American Society of Engineers (ASCE)–American Concrete Institute (ACI) Joint Committee 426,[1] the two primary forms of shear cracking in prestressed concrete components are web-shear and flexure-shear cracking. Web-shear cracks are diagonal cracks that first develop in the region of greatest shear and propagate diagonally outward with increasing load. Flexure-shear cracks develop as diagonal extensions of flexural cracks. The width, spacing, and angle of web-shear cracks and flexure-shear cracks as a function of load and stress level are important aspects of the behavior of prestressed concrete components.

Accurate prediction of the load that causes all forms of cracking is important because the onset of cracking changes the load-carrying mechanism of the precast concrete component and because cracking can lead to long-term strength reduction due to the corrosion or fatigue of reinforcement. The flexural cracking load of a prestressed concrete member can be calculated as a function of the cracking strength of concrete, the initial prestressing force, and the losses in prestressing force due to elastic shortening, creep, and shrinkage. The web-shear crack-

ing load is typically calculated based on Mohr's circle of stress at the location of the neutral axis with consideration of the longitudinal stress due to prestressing. The mechanism of flexure-shear cracks is more complicated and is not entirely understood. Empirical approaches have been developed for estimating flexure-shear cracking strengths that are based on the statistical analysis of test data from several researchers.[2–4]

It is also important to be able to accurately estimate the angle of diagonal cracking because it is a good indicator of how many stirrups participate in lifting the diagonal compressive force above an inclined crack. From this determination of stirrup participation, a reliable contribution of shear reinforcement to capacity is able to be calculated.[5,6] Significant research has been completed to examine the factors that influence the angle of cracking in concrete panels and elements,[7,8] but significantly less research is available for examining shear-crack angles in flexural members. This insufficiency is partly due to the difficulty of recording and analyzing the complex crack patterns in beam tests. The traditional hand-drawn crack-recording method is time-consuming and does not always provide reliable or complete crack maps. To overcome these deficiencies, a few researchers have applied close-range, digital photogrammetry methods to record the development of cracks,[9,10] and these techniques have proved to be efficient and reliable.

The crack-width rate of growth is also important for evaluating the durability of structures in different environments. To enable the consideration of cracking in design, codes of practice provide relationships for estimating crack widths. *Building Code Requirements for Structural Concrete (ACI 318-05) and Commentary (ACI 318R-05)*[11] adopts the Gergely-Lutz crack-width equation[12] that is derived statistically from a series of tests. The Euro-International Concrete Committee (CEB)–International Federation for Prestressing (FIP) *Model Code for Concrete Structures: CEB-FIP International Recommendations*[13] provides an expression for calculating crack spacing and suggests that the crack width can be calculated as the difference in the elongation of the steel and the concrete over this crack spacing.

There are several other empirical formulas for calculating crack widths.[14,15,16] Because these expressions are based on flexural or uniaxial tension tests, it is uncertain if these formulas will provide reasonable estimates of crack spacing and widths in the shear regions of prestressed concrete members. This is because prestressed concrete members are in a more complex state of stress in which the reinforcement is not aligned with the direction of cracking.

The tensile strength of concrete, which increases with increasing compressive strength, has a significant influence on the cracking behavior of a member that goes beyond its influence on initial cracking loads. In members cast with high-strength concrete (HSC), cracks typically propagate through aggregates, which produces smoother and flatter cracks.

In addition, there is a greater release of elastic strain energy with cracking in HSC structures due to the greater fracture (tensile) strengths in these concretes. This can lead to the more rapid propagation of cracks, more widely spaced and wider cracks, and greater energy transfer to the reinforcement that crosses the cracks. Coupled with the improved bond between reinforcement and HSC, this can lead to local yielding of reinforcement at crack locations at the first occurrence of cracking.[17] Current methods for predicting cracking behavior, however, are based on tests for normal-strength concrete components.

As part of a project sponsored through the National Cooperative Highway Research Program (NCHRP) and conducted at the University of Illinois at Urbana-Champaign, 20 shear tests were conducted on 73-in.-deep (1850 mm) or 63-in.-deep (1600 mm) HSC bulb-tee girders. In this project, a crack-recording method was developed based on digital, close-range photogrammetry to accurately track the development of cracking.

This paper describes this crack-recording method and presents a summary of the measured cracking of test girders. The measured values are compared with predictions using current methods for cracking strength, crack angles, crack spacing, and crack widths. The significance of these results is also discussed, and equations for computing the average spacing and maximum crack width of inclined cracks are proposed to overcome the unconservative results of current methods for these types of members.

Experimental test program

Ten prestressed concrete bulb-tee girders were cast with HSC. The nomenclature used to label the girders includes one number between two letters. The first letter, G, stands for *girder*; the number refers to the number of the girder; and the final letter, an E or a W, indicates the east or west half of each girder. Each girder was 73 in. (1850 mm) deep and 52 ft (16 m) long. The composite section was composed of a 63-in.-deep (1600 mm) bulb-tee girder and a 42-in.-wide × 10-in.-thick (1100 mm × 250 mm) deck. The compressive strength of the concrete in these girders ranged from 9.6 ksi to 17.8 ksi (66 MPa to 123 MPa).

Seven-wire, 0.6-in.-diameter (15 mm), low-relaxation prestressing strands were used for all girders. All transverse reinforcement was ASTM A615[18] Grade 60 (420 MPa) deformed steel bars except for the deformed welded-wire reinforcement in G5E. **Table 1** presents the details of the test girders. Two shear-failure results were obtained from each test by repairing the first failed end and then reloading until the capacity of the other end was reached.

Table 1. Summary of experimental research program for 63-in.-deep bulb-tee girders

Girder end	f'_c, ksi	Strands		f_{pe}, ksi	$\rho_v f_y$, ksi	Shear reinforcement		
		Bottom	Top			Section 1	Section 2	Section 3
G1E	12.1	32S	2S	159.7	0.39	Two no. 4 × 12 in.	Two no. 4 × 24 in.	n.a.
G1W	12.1	26S + 6P	2S	159.7	0.39	Two no. 4 × 12 in.	Two no. 4 × 24 in.	n.a.
G2E	12.6	38S	2S	150.2	0.75	Two no. 5 × 11 in.	Two no. 5 × 17 in.	Two no. 4 × 22 in.
G2W	12.6	32S + 6P	2S	150.2	0.75	Two no. 5 × 11 in.	Two no. 5 × 17 in.	Two no. 4 × 22 in.
G3E	15.9	42S	2S	154.9	0.57	Two no. 4 × 8 in.	Two no. 4 × 12 in.	Two no. 4 × 24 in.
G3W	15.9	42S	2S	154.9	0.57	Two no. 4 × 8 in.	Two no. 4 × 12 in.	Two no. 4 × 24 in.
G4E	16.3	42S	2S	153.7	1.11	Two no. 5 × 6 in.	Two no. 5 × 10 in.	Two no. 5 × 24 in.
G4W	16.3	42S	2S	153.7	1.11	Two no. 5 × 6 in.	Two no. 5 × 10 in.	Two no. 5 × 24 in.
G5E	17.8	24S	n.a.	174.7	0.17	Two D11 × 20 in.*	n.a.	n.a.
G5W	17.8	24S	n.a.	174.7	0.14	Two no. 3 × 20 in.	n.a.	n.a.
G6E	12.7	42S	2S	167.6	0.56	Two no. 5 × 12 in.	Two no. 5 × 20 in.	Two no. 3 × 24 in.
G6W	12.7	42S (18D)	2S	167.6	0.56	Two no. 5 × 12 in.	Two no. 5 × 20 in.	Two no. 3 × 24 in.
G7E	12.5	42S	2S	167.0	0.58	Two no. 4 × 8 in.	Two no. 4 × 12 in.	Two no. 4 × 24 in.
G7W	12.5	42S	2S	167.0	0.58	Two no. 4 × 8 in.	Two no. 3 × 23 in.	n.a.
G8E	13.3	42S	2S	158.5	0.58	Two no. 4 × 8 in.	Two no. 4 × 12 in.	Two no. 4 × 24 in.
G8W	13.3	42S	2S	158.5	0.58	Two no. 4 × 8 in.	Two no. 4 × 12 in.	Two no. 4 × 24 in.
G9E	9.6	34S	2S	166.5	1.04	Two no. 5 × 6.5 in.	Two no. 4 × 7.5 in.	Two no. 4 × 24 in.
G9W	9.6	26S + 8P	2S	166.5	1.69	Two no. 5 × 4 in.	Two no. 4 × 7.5 in.	Two no. 4 × 24 in.
G10E	10.6	34S (8D)	2S	173.7	0.75	Two no. 5 × 9 in.	Two no. 4 × 10 in.	Two no. 4 × 22 in.
G10W	10.6	26S + 8P	2S	173.7	0.75	Two no. 5 × 9 in.	Two no. 4 × 10 in.	Two no. 4 × 22 in.

* Two layers of welded-wire reinforcement were used (20 × 20 by D11 × D11 [500 × 500 by MD71 × MD71]).

Note: D = debonded strands; f'_c = specified compressive strength of concrete; f_{pe} = compressive stress in concrete due to effective prestressing forces only at extreme tensile fiber of section; f_y = stress and yield strength of reinforcement; P = draped strands; S = straight strands; ρ_v = shear reinforcement ratio. 1 in. = 25.4 mm; 1 ksi = 6.895 MPa.

All test girders were simply supported over a 50 ft (15 m) span and subjected to a uniformly distributed load. The distributed load was imposed by 44 hydraulic jacks spaced 1 ft (0.3 m) apart over the central 44 ft (13.4 m) of the span.

During each test, the load was paused at several intervals, which were called load stages, so that discrete measurements could be taken, cracks could be marked and their widths measured, and photographs taken to record the state of crack development. For each pause in loading, 20 to 40 photographs were taken, producing several hundred photographs per test. Using the principles of digital, close-range photogrammetry, a crack-recording method was developed to extract the crack information stored in those pictures to track the development of cracking in an efficient and accurate manner.

Crack-recording method

Figure 1 schematically illustrates the seven-step procedure used in the crack-recording method. Following is a list of the steps:

1. **Image acquisition** After a picture was taken, it was saved in digitized format as a gray-level image. Color images were converted to gray-level images for further image processing.

2. **Crack enhancement** All cracks in the picture were highlighted in white to ensure that the crack contrasted sharply with the background.

3. **Crack detection** The edge-detection techniques of image processing[19] were applied to obtain the crack positions in the image coordinate.

4. **Camera calibration** The camera parameters, both intrinsic parameters (such as focal length) and extrinsic parameters (such as the object position of camera), were derived from the process of camera calibration. This calibration was achieved using a number of points on the girder surface. The points had known locations in world coordinates, and the image coordinates of the points were measured in the image. Those points are called control points. In this project, Zurich (also known as Demec) targets were distributed over the surface of the web in a 10 in. (254 mm) grid and treated as control points. The new two steps of camera calibration[20] were adopted in this research.

5. **Coordinate transformation** Once the camera parameters were determined, the crack locations in the real, three-dimensional world were obtained by converting the image coordinates to world coordinates by executing the coordinate algorithm.[21]

6. **Error elimination** The step of error elimination minimized the errors produced in the transformation due to either the approximation of the camera parameters or the inaccuracy of the measurements on the positions of control points.

7. **Crack merging** By applying the previous six steps to each picture, the crack information was collected for that load stage. The last step, crack merging, created the entire crack pattern from individual images.

An evaluation illustrated that the locations of the cracks were measured to an accuracy of 0.1 in. (2.5 mm).

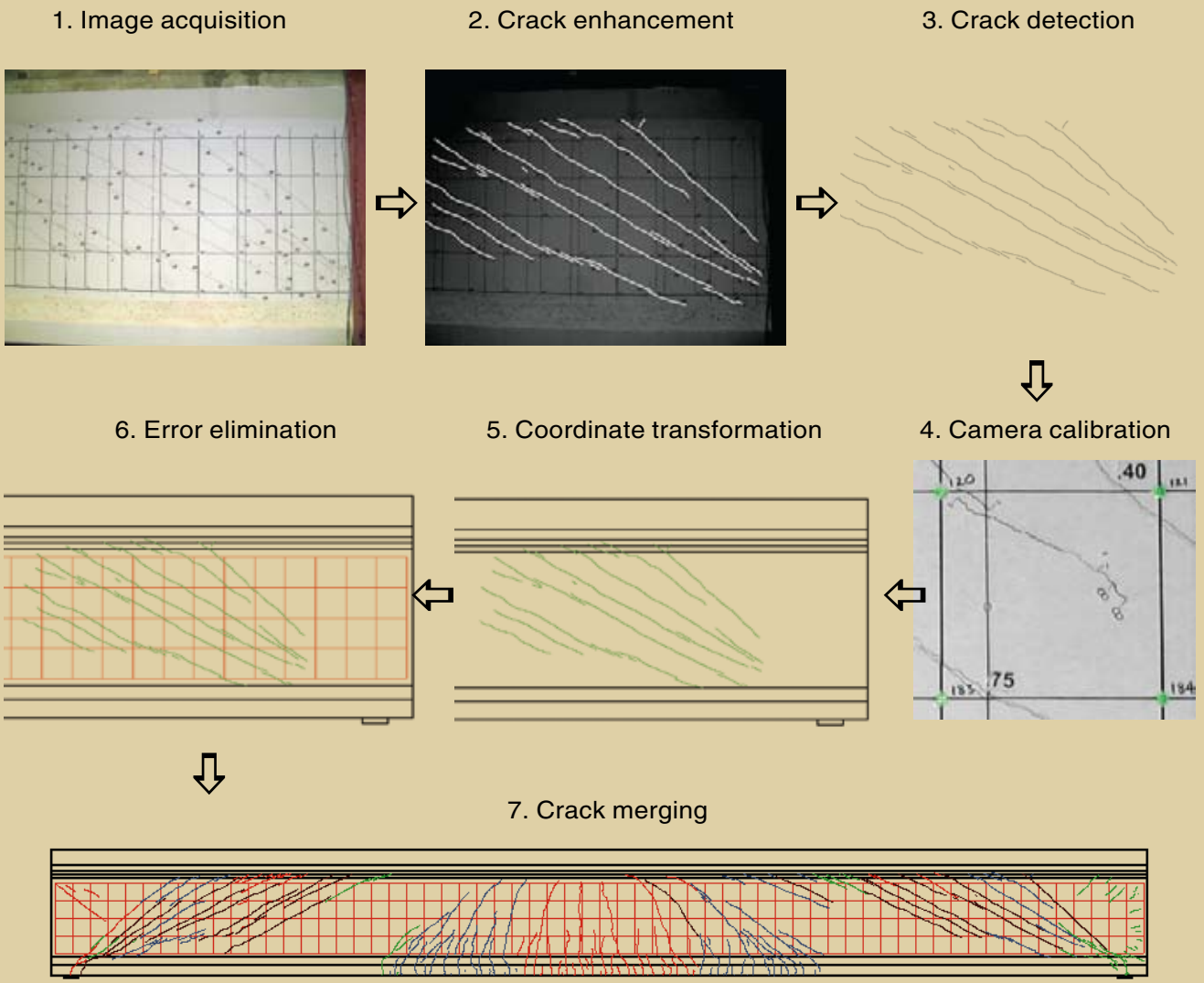

Figure 1. This diagram shows the steps of the crack-recording procedure.

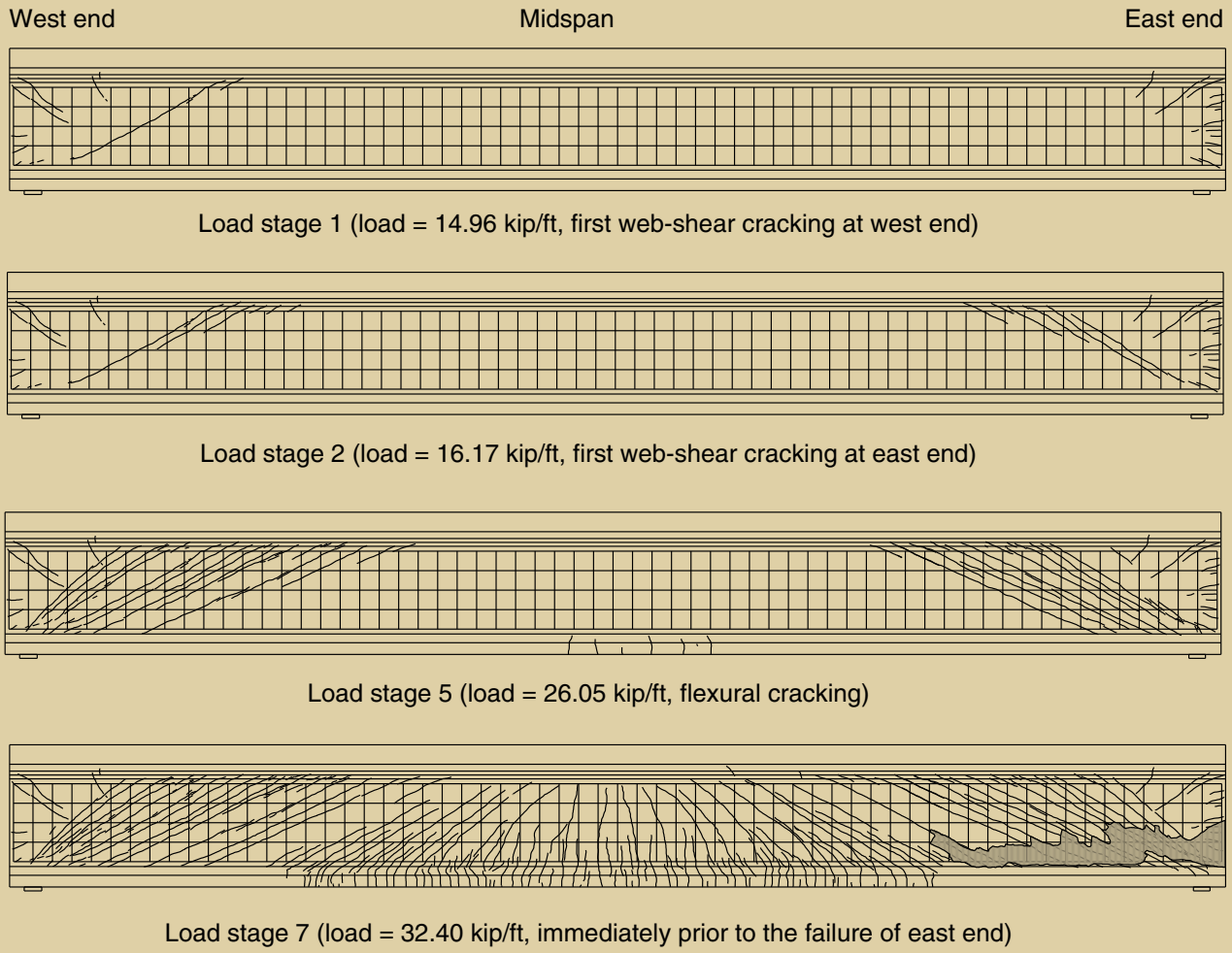

Figure 2. These drawings illustrate the crack pattern of girder 3. Note: 1 kip/ft = 14.6 kN/m.

Crack development and pattern

Figure 2 shows an example of the development of cracking as measured in girder 3. This pattern of development was similar to that of other girders. Prior to loading, spalling cracks appeared in the extreme ends of most members. These initial cracks were due to the tensile stresses caused by anchoring of the strands in the bottom bulb. They did not propagate further during the loading and typically decreased in width with loading.

The first cracks to occur in all members were web-shear cracks in the end regions of the members. Nearly all of these first cracks, and most other web-shear cracks, occurred with a loud popping sound. Under increasing load, additional web-shear cracks occurred, typically farther from the support. The majority of the web-shear cracks developed over the full height of the girder at the same time and with an audible sound.

Figure 2 shows the onset of flexural cracking at midspan. As the loading continued beyond this point, existing flexural cracks propagated upward while new flexural and shear cracks developed. By contrast, with the web-shear cracking the development of the flexure and flexure-shear cracks was incremental and quieter. In the flexural region farther from midspan, the effect of the shear force caused the initial flexural cracks to grow into flexure-shear cracks.

As the load increased, the widths of existing cracks also increased. The level of prestressing and the magnitude of design shear stress influenced the extent of shear cracking over the length of the girder. For members designed for greater design shear stresses, the webs of the girders became heavily cracked over their entire length and the bottom bulbs developed cracks to within a few feet of the support. In some of the girders designed for large shear stresses, a nearly stable crack pattern developed, after which cracks only widened with increasing load.

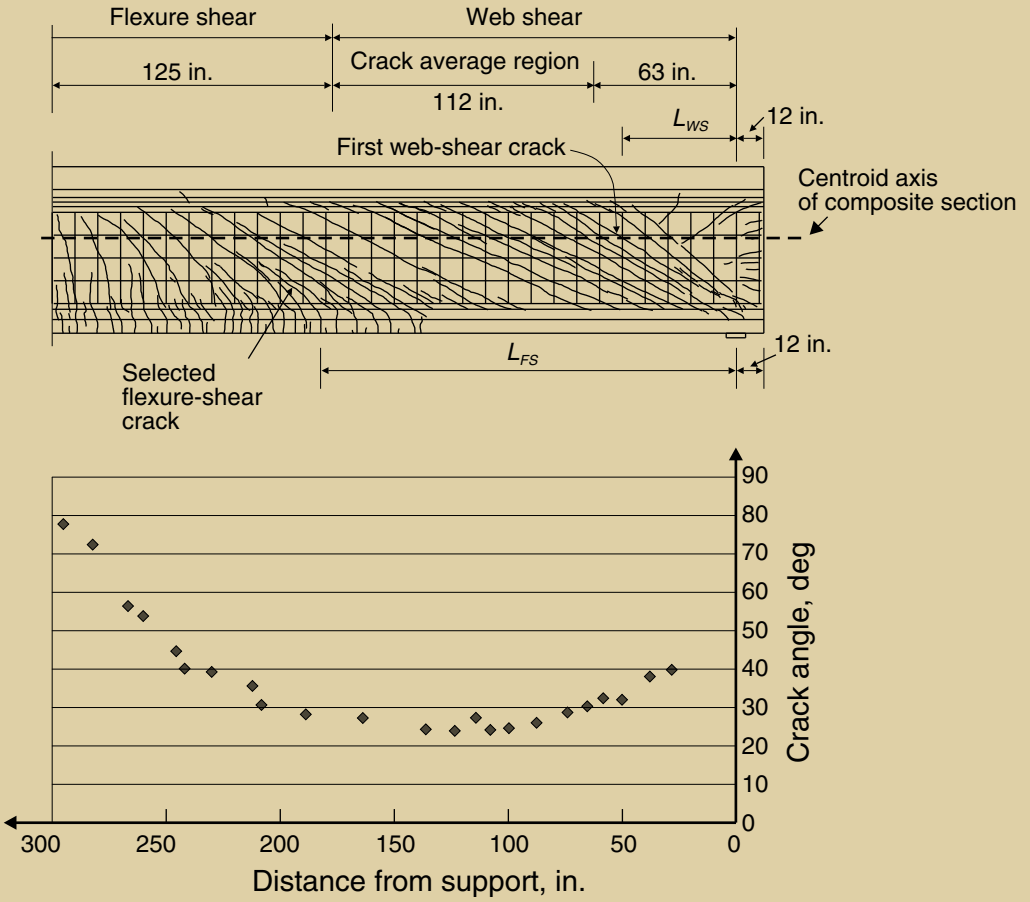

Figure 3. This figure shows the crack-angle distribution of the east end of girder 1. Note: L_{FS} = location of evaluated flexure-shear crack measured from the support; L_{WS} = location of first web-shear crack measured from the support. 1 in. = 25.4 mm.

Crack angle

As illustrated in Fig. 2, it is reasonable to characterize shear cracks as straight lines with one slope or angle. In this research, a least-squares procedure was used to find the average angle for each crack. Only the crack profiles within the web were considered when assessments were made of the angle of best fit for each crack.

Figure 3 illustrates an example of making this assessment of crack angle for G3E. The longitudinal position of each crack was taken as the point at which each crack crossed the centroidal axis of the composite section. When the crack angle is plotted against the distance from the support, the shape of the line that passes through the measured points is parabolic (Fig. 3). For G3E, the crack angle was approximately 45 deg near the support. It then decreased to 25 deg in the first shear-design region (about $d_v\cot\theta$ from support, where d_v is the effective shear depth and θ is the crack angle), increased again to 45 deg in the flexure-shear cracking zone, and then increased to the expected 90 deg angle near midspan, where only flexural cracking occurred.

Similar patterns occurred in the other girders. For girders designed with greater shear stresses, such as girders 4 and 9, the cracking was extensive and the crack-angle data points illustrated a clear parabolic pattern.

Crack spacing

The measured pattern of cracking was also used to assess the average spacing of cracks. The horizontal spacing S_x, or the horizontal distance between any two adjacent cracks, can be computed from their positions on the x-axis. Furthermore, the spacing of any two adjacent cracks S was computed from S_x and the crack angle θ as S is equal to $S_x\sin\theta$. **Table 2** lists the average values of measured spacing S_x and calculated spacing S of web-shear cracks along the centroidal axis of the composite section for all tests.

The derivation of modified compression field theory[22] suggested an empirical equation (Eq. [1]) for computing the average spacing of the inclined cracks S.

Table 2. Average spacing of web-shear cracks

Girder end	d_b/ρ_v, in.	Test			$\frac{S_{test}}{S_{CEB}}$	$\frac{S_{test}}{S_{Eq.(5)}}$
		S_x, in.	S, in.	$S\cos\theta$, in.		
G1E	90.0	13.7	6.6	5.7	0.52	1.33
G1W	90.0	7.3	3.6	3.1	0.28	0.72
G2E	66.5	11.6	5.7	4.9	0.52	1.31
G2W	66.5	7.7	4.0	3.4	0.36	0.89
G3E	60.0	8.8	4.4	3.7	0.43	1.15
G3W	60.0	9.1	4.5	3.8	0.54	1.16
G4E	36.3	6.6	3.5	2.9	0.42	1.04
G4W	36.3	5.9	3.2	2.7	0.47	0.93
G5E	204.5	12.8	6.0	5.1	0.29	0.98
G5W	204.5	14.1	6.7	5.8	0.33	1.08
G6E	90.0	10.1	4.8	4.2	0.42	0.98
G6W	90.0	10.2	5.4	4.4	0.46	1.12
G7E	60.0	9.5	4.4	3.6	0.43	1.08
G7W	60.0	8.5	3.8	3.4	0.37	0.94
G8E	60.0	8.0	4.0	3.4	0.39	0.98
G8W	60.0	9.9	5.0	4.3	0.49	1.22
G9E	39.3	8.0	4.2	3.5	0.49	1.10
G9W	24.2	5.6	3.1	2.6	0.43	0.88
G10E	54.4	7.7	4.1	3.4	0.41	0.97
G10W	54.4	8.6	4.6	3.9	0.46	1.10
Average					0.42	1.03
Coefficient of variation					0.17	0.14

Note: d_b = bar diameter; S = average crack spacing of the inclined cracks; S_{CEB} = calculated spacing by CEB-FIP approach;[13] $S_{Eq.(5)}$ = calculated spacing using Eq. (5) proposed in this paper; S_{test} = measured spacing; S_x = average crack spacing measured in the longitudinal (x) direction; θ = crack angle; ρ_v = shear reinforcement ratio. 1 in. = 25.4 mm.

$$S = \frac{1}{\left(\frac{\sin\theta}{s_{mx}} + \frac{\cos\theta}{s_{mv}}\right)} \quad (1)$$

where

s_{mx} = average crack spacing due to longitudinal tension

s_{mv} = average crack spacing due to transverse tension

Equation (2), suggested by the CEB-FIP code to calculate average crack spacing s_m, provided the calculations for s_{mx} and s_{mv}.

$$s_m = 2\left(c + \frac{s}{10}\right) + k_1 k_2 \frac{d_b}{\rho_{ef}} \quad (2)$$

where

c = concrete cover

s = maximum spacing between reinforcing bars

k_1 = coefficient for the bond properties of the bar

k_2 = coefficient to account for the strain gradient

d_b = bar diameter

ρ_{ef} = effective reinforcement ratio

Table 2 compares the measured crack spacing with that calculated by Eq. (1). In the prediction, k_1 was taken 0.4 for deformed bars, and k_2 was taken as 0.25. These comparisons illustrated that the average measured spacing was about half of the value calculated using the CEB-FIP expression for s_m.

Due to the inaccuracy of this method, the authors developed another approach for calculating the spacing of inclined cracks. It was derived by considering the resistance mechanisms in an inclined crack surface before and immediately after the onset of cracking. Before cracking, the tensile force perpendicular to the potential crack surface is calculated with the following equation.

$$\frac{f_{ct} b_w h_w}{\sin\theta}$$

where

f_{ct} = concrete tensile strength

b_w = web width

h_w = crack depth

At these small levels of tensile strain, it was considered reasonable to neglect the contribution of the steel reinforcement before cracking. Immediately after cracking, the tensile force was resisted by the component of tensile force in stirrups in the same direction, as indicated in Eq. (3).

$$\frac{f_{ct} b_w h_w}{\sin\theta} = f_s A_v \cos\theta \tag{3}$$

where

f_s = mild-steel reinforcement stress

A_v = area of stirrups across the crack

The mild-steel reinforcement stress f_s is a function of the bond stress f_b, the bar diameter d_b, and the bond length l_b as calculated in the next equation.[23]

$$f_s = \frac{4 l_b f_b}{d_b}$$

Furthermore, the bond length is a function of the vertical-crack spacing S_y.

$$l_b = 0.5 S_y$$

where

$$S_y = \frac{S}{\cos\theta}$$

The area of the stirrups across the crack can be determined from the next equation.

$$A_v = \rho_v b_w h_w \cot\theta$$

where

ρ_v = shear reinforcement ratio

With these substitutions, the crack spacing can be derived from Eq. (3) as Eq. (4).

$$S\cos\theta = \frac{1}{2}\frac{f_{ct}}{f_b}\frac{d_b}{\rho_v} \tag{4}$$

Equation (4) was modified to become Eq. (5) to provide an empirical expression that gave a good fit with the experimental test data.

$$S\cos\theta = c_1 + \left(c_2 - c_3 f_c'\right)\frac{d_b}{\rho_v} \tag{5}$$

where

c_1 = constant coefficient for crack spacing

c_2 = constant coefficient for crack spacing

c_3 = constant coefficient for crack spacing

f_c' = specified compressive strength of concrete

The values of c_1, c_2, and c_3 that were the best fit were based on measured values of f_c' from Table 1 and d_b/ρ_v and $S\cos\theta$ from Table 2 using the least-square method. This yielded values for c_1 of 2.3 in. (58 mm), c_2 of 0.04, and c_3 of 0.00135/ksi. Table 2 also compares the measured crack spacing with the calculated values using Eq. (5). The mean ratio of measured crack spacing to calculated crack spacing was 1.03 with a coefficient of variation *COV* of 0.14.

Table 3. First web-shear cracks and average angle for the web-shear cracks

Girder end	First cracking							Average cracking angle		
	Load, kip/ft	L_{WS}, in.	θ_{test}, deg	f_{pc}, psi	$\frac{V_{test}}{V_{cw}}$	$\frac{\theta_{test}}{\theta_{Mohr}}$	$\frac{\theta_{test}}{\theta_{FEA}}$	θ_{test}, deg	$\frac{\cot\theta_{test}}{\cot\theta_{Mohr}}$	$\frac{\cot\theta_{test}}{\cot\theta_{LRFD}}$
G1E	14.7	41.2	43.0	907	1.17	1.45	1.31	26.7	1.11	0.85
G1W	18.1	120.9	30.0	1086	0.86	1.06	1.07	28.4	0.98	0.86
G2E	18.5	47.0	38.0	904	1.45	1.27	1.26	28.5	1.05	0.88
G2W	21.7	64.7	37.0	1104	1.29	1.31	1.34	30.9	0.90	0.88
G3E	16.1	50.1	38.0	1224	1.02	1.34	1.25	26.1	1.06	0.90
G3W	15.0	71.4	28.0	1236	0.86	0.99	0.97	27.1	1.02	0.86
G4E	14.3	57.1	35.0	1037	0.94	1.17	1.17	28.7	1.00	0.99
G4W	15.4	63.3	34.0	1041	0.99	1.14	1.16	30.7	0.93	0.91
G5E	16.8	40.3	43.0	528	1.38	1.22	1.14	23.7	1.53	0.91
G5W	12.2	55.6	35.0	539	0.94	0.99	0.99	25.6	1.40	0.83
G6E	16.2	66.4	38.0	930	1.15	1.28	1.40	28.2	1.02	0.82
G6W	16.7	31.3	46.0	453	1.70	1.31	1.27	26.4	1.27	0.98
G7E	17.9	55.6	32.0	1058	1.27	1.12	1.12	25.8	1.04	0.93
G7W	18.9	48.7	38.0	1053	1.38	1.33	1.28	25.5	1.06	0.94
G8E	14.5	53.6	36.0	839	1.12	1.17	1.29	27.7	1.03	0.84
G8W	15.7	59.7	33.0	844	1.18	1.07	1.18	28.3	1.00	0.82
G9E	16.0	56.0	35.0	941	1.30	1.23	1.25	28.5	0.99	1.19
G9W	21.6	52.7	35.0	1101	1.48	1.29	1.31	32.2	0.81	0.92
G10E	15.6	55.3	35.0	759	1.36	1.14	1.19	29.4	0.99	0.98
G10W	19.3	40.1	35.0	1092	1.34	1.27	1.26	28.3	0.94	0.97
Average					1.21	1.21	1.21	n.a.	1.06	0.91
Coefficient of variation					0.19	0.10	0.09	n.a.	0.16	0.09

Note: f_{pc} = compressive stress at centroid of composite section; L_{WS} = location of first web-shear crack measured from the support; V_{cw} = web-shear cracking strength; V_{test} = measured sectional shear force; θ = crack angle; θ_{FEA} = crack angle determined by nonlinear finite-element analysis; θ_{LRFD} = crack angle determined by *AASHTO LRFD Bridge Design Specifications*; θ_{Mohr} = crack angle determined using Mohr's circle of stress; θ_{test} = crack angle determined by testing. 1 in. = 25.4 mm; 1 kip/ft = 14.6 kN/m; 1 psi = 6.895 kPa.

Web-shear cracking

First web-shear cracking

The occurrence of the first diagonal crack is a significant event in the life of a structure because it signifies the point at which stirrups begin to significantly participate in the response and when fatigue needs be considered. The estimation of cracking load is often desirable, and the aim of some states is to keep prestressed concrete members uncracked under service loads in order to enhance the durability of these structures.

Equation (6) presents an expression for web-shear cracking strength V_{cw} as provided by the American Association of State Highway and Transportation Officials' (AASHTO's) *Standard Specifications for Highway Bridges*.[24]

$$V_{cw} = \left(3.5\sqrt{f_c'} + 0.30 f_{pc}\right) b_w d + V_p \quad (6)$$

where

f_{pc} = compressive stress at centroid of composite section

d = distance from extreme compression fiber to centroid of longitudinal tension reinforcement

V_p = vertical component of effective prestressing force at a section

Equation (6) was derived from the Mohr's circle of stress with the state of stress taken as that at the centroidal axis of the girder and the tensile-cracking strength of the concrete taken as about $4\sqrt{f_c'}$.

During the test, the first load stage ended when the first audible web-shear crack occurred. It was also possible to verify the first cracking load by the sudden increase in stirrup strains.

First diagonal cracking often involved the development of two or three simultaneous cracks. **Table 3** summarizes the measured web-shear cracking loads and the locations of the first web-shear crack L_{WS}, measured from the center of the support along the centroid of the composite section (Fig. 3). First cracks occurred at a distance less than one girder depth of 73 in. (1850 mm) from the center of the support for all tests except G1W.

Table 3 compares the web-shear cracking loads calculated by AASHTO standard specifications $V_{cw,STD}$ with the measured cracking loads V_{test}. The mean of the shear strength ratios $V_{test}/V_{cw,STD}$ was 1.21 with a *COV* of 0.19. The AASHTO standard specifications expression for V_{cw} provided a conservative and reasonably accurate prediction of the first web-shear cracking strength, particularly considering the natural variability of concrete tensile cracking strength.

In calculating the V_{cw} presented in Table 3, the full effective prestressing force was used for f_{pc}, and d was taken as the distance from the top of the deck to the centroid of the strands in the bottom half of the girder. The value of d was usually larger than 63 in. (1600 mm). Because the first crack occurred close to the support and the prestressing strands were anchored in the bottom of the member, the actual f_{pc} at mid-depth was expected to be somewhat less than the calculated values, yet the expression for V_{cw} was typically conservative. The apparent contradiction suggests that the principal tensile stress was greater than $4\sqrt{f_c'}$, the shear forces carried by the top flange and the bottom bulb were not negligible, or both.

Crack angle of first web-shear cracking

Table 3 also presents the measured and calculated angles of diagonal cracking. The predicted angle of diagonal cracking was calculated using Mohr's circle of stress θ_{Mohr} and the full magnitude of f_{pc} as given in Eq. (7).

$$\cot\theta = \sqrt{1 + \frac{f_{pc}}{f_t}} \quad (7)$$

where

f_t = concrete tensile strength

$= 4\sqrt{f_c'}$

The angle of diagonal cracking θ_{FEA} was also predicted using the results from a nonlinear finite-element analysis.

The mean ratio of crack angle of diagonal cracking from testing to crack angle determined by Mohr's circle of stress $\theta_{test}/\theta_{Mohr}$ was 1.21 with a *COV* of 0.10. This high mean was expected due to the likely overestimation of f_{pc}. The mean ratio of $\theta_{test}/\theta_{FEA}$ was 1.21 with a *COV* of 0.09. There was a close correlation between the measured and the predicted values.

Average cracking angle in web-shear design region

For calculating the shear reinforcement contribution to capacity, the most important angle of web-shear cracking was the dominant crack in the first shear design span extending for a distance of about $d_v\cot\theta$ from the support. Figure 3 illustrates that the angle of diagonal cracking for much of this design shear span was reasonably constant. Table 3 presents the average angle of web-shear cracking in the first design region (Fig. 3) for each girder end. Equation (7) was used for predicting the crack angle in this region for which it was reasonable to expect that the prestressing was fully effective.

The mean ratio of $\cot\theta_{test}/\cot\theta_{Mohr}$ for this first shear design span was 1.06 with a *COV* of 0.16. This method provided a reasonable and conservative prediction of the crack angle with the exception of those for girders 5 and 6. Table 3 compares the measured web-shear crack angles with the angles of diagonal compression from Table 5.8.3.4.2-1 of the *AASHTO LRFD Bridge Design Specifications*.[25] The mean ratio of $\cot\theta_{test}/\cot\theta_{LRFD}$ was 0.91 with a *COV* of 0.09. This implies that the AASHTO LRFD specifications rely on the shear stress's being transmitted across a crack to achieve a flatter angle of diagonal compression.

The comparisons of the angles of cracking in the web-shear region are useful for assessing the appropriateness and conservatism of standard codes of practice for calculating the contribution of shear reinforcement. Both AASHTO standard specifications and ACI 318-05 calculate the contribution of the shear reinforcement using the number of stirrups that are calculated to cross a 45 deg crack (s/d). This method was found to be highly

Table 4. Flexure-shear cracks

Girder end	Position L_{FS}, ft	Test				STD		M/M_{cr}	V/V_{ci}
		Angle, deg	Load, kip/ft	M, kip-ft	V, kip	M_{cr}, kip-ft	V_{ci}, kip		
G1E	17.7	51.3	24.1	6786	177	5628	182	1.21	0.97
G1W	14.7	46.4	26.3	6718	271	5389	256	1.25	1.06
G2E	12.5	34.6	26.8	6152	336	6340	389	0.97	0.87
G2W	12.2	39.0	26.8	6050	344	5996	383	1.01	0.90
G3E	15.2	39.4	28.6	7439	281	6997	307	1.06	0.92
G3W	16.0	42.8	28.6	7649	259	6986	278	1.09	0.93
G4E	10.7	31.3	31.8	6544	455	7270	553	0.90	0.82
G4W	11.1	30.2	31.0	6553	432	7262	526	0.90	0.82
G5E	13.4	31.1	16.6	3991	193	5223	299	0.76	0.64
G5W	18.6	59.8	20.0	5738	128	5151	157	1.11	0.82
G6E	14.4	35.8	34.1	6255	289	7892	558	0.79	0.74
G6W	15.1	39.6	34.1	6257	411	5615	414	1.11	0.99
G7E	16.1	38.0	31.9	8538	285	7690	294	1.11	0.97
G7W	13.1	37.0	32.2	7650	383	7738	429	0.99	0.89
G8E	16.0	39.9	35.5	7721	288	7535	320	1.02	0.90
G8W	16.8	36.2	35.5	8792	234	7524	238	1.17	0.98
G9E	12.1	35.0	23.5	5265	304	6116	393	0.86	0.77
G9W	13.1	41.4	24.3	5752	290	5993	340	0.96	0.85
G10E	14.6	46.2	22.9	5816	237	5338	255	1.09	0.93
G10W	17.4	60.8	22.0	6139	168	6413	210	0.96	0.80
Average								1.02	0.88
Coefficient of variation								0.13	0.11

Note: L_{FS} = location of evaluated flexure-shear crack measured from the support; M = moment; M_{cr} = moment-causing flexural cracking at section; STD = *AASHTO Standard Specifications for Highway Bridges*; V = shear force; V_{ci} = flexure-shear cracking strength. 1 ft = 0.305 m; 1 kip = 4.448 kN.

conservative for determining the number of stirrups that lift the diagonal compressive force across a crack. If the measured angle of cracking from these experiments is used for evaluating the contribution of stirrups, then typically at least twice this number of stirrups (cot[26.2] = 2) should be considered in evaluating the shear capacity of reinforcement V_s.

The AASHTO LRFD specifications were found in many instances to consider a larger number of stirrups in evaluating the shear capacity of the reinforcement V_s than the number that were observed to cross the identified critical shear crack. The AASHTO LRFD specifications method may be unconservative (Table 3). Another approach for evaluating the contribution of the shear reinforcement was taken with the new simplified shear-design provisions[6] that have been added to the fourth edition of the AASHTO LRFD specifications. According to these provisions, the contributions of transverse shear reinforcement are calculated using the angle of diagonal cracking calculated by Mohr's circle of stress.

Flexure-shear cracking

Flexure-shear cracks develop from the extension of flexural cracks in regions of high flexure and significant shear. In the AASHTO standard specifications, the flexure-shear cracking strength V_{ci} was calculated by Eq. (8).

Table 5. Flexure cracks and flexural cracking moment

Girder	Test			STD		$\frac{\varepsilon_{test}}{\varepsilon_{STD}}$	$\frac{M_{cr,test}}{M_{cr,STD}}$
	Load,* kip/ft	$\Delta\varepsilon$ † × 10^{-6}	M_{cr},‡ kip-ft	$\Delta\varepsilon$ × 10^{-6}	M_{cr}, kip-ft		
G1	19.6	661	6025	783	6386	0.84	0.94
G2	21.6	683	6642	757	7158	0.90	0.93
G3	23.1	725	7127	962	7984	0.75	0.89
G4	26.3	668	8094	957	10,081	0.73	0.83
G5	16.8	509	5159	696	5734	0.73	0.90
G6	23.7	703	7299	1090	8878	0.65	0.82
G7	23.3	808	7167	1299	8795	0.62	0.81
G8	25.7	803	7916	1244	8662	0.65	0.91
G9	20.2	634	6225	866	6771	0.73	0.92
G10	20.0	777	6163	1094	7308	0.71	0.84
Average						0.73	0.88
Coefficient of variation						0.12	0.06

* Distributed load at first flexural cracking.
† Average strain measured by the bottom linear variable displacement transducer.
‡ Corresponding cracking moment.

Note: M_{cr} = moment causing flexural cracking at section; $M_{cr,STD}$ = flexural cracking moment determined by the American Association of State Highway and Transportation Officials' (AASHTO's) *Standard Specifications for Highway Bridges*; $M_{cr,test}$ = measured flexural-cracking moment; STD = AASHTO standard specifications; $\Delta\varepsilon$ = strain increment; ε_{STD} = strain determined by AASHTO standard specifications; ε_{test} = measured strain. 1 ft = 0.305 m; 1 kip = 4.448 kN.

$$V_{ci} = 0.6\sqrt{f_c'}\,b_w d + V_d + \frac{V_i M_{cr}}{M_{max}} \qquad (8)$$

where

V_d = shear force at section due to self-weight

V_i = shear force at section due to externally applied load

M_{max} = maximum moment at section due to externally applied load

M_{cr} = moment causing flexural cracking at section

$$= \left(\frac{I}{y_t}\right)\left(6\sqrt{f_c'} + f_{pe} - f_d\right)$$

where

I = moment of inertia of section

y_t = distance from centroidal axis of gross section to extreme fiber in tension

f_{pe} = compressive stress in concrete due to effective prestressing forces only at extreme tensile fiber of section

f_d = stress due to self-weight at extreme tensile fiber of section

In this relationship, V_{ci} consists of three components. The sum of the latter two is the shear force corresponding to flexural cracking, and the first term is the increment in shear force expected to form a shear crack from a flexure crack. When computing the flexure-shear strength, the flexural cracking stress is taken as $6\sqrt{f_c'}$.

As the test load increased, the flexure-shear cracks extended from the end of the web-shear cracking region to near midspan. A rapid change in the stirrup strain-gauge readings identified the occurrence of flexure-shear cracking. For each half of the girder, one flexure-shear crack was examined in detail.

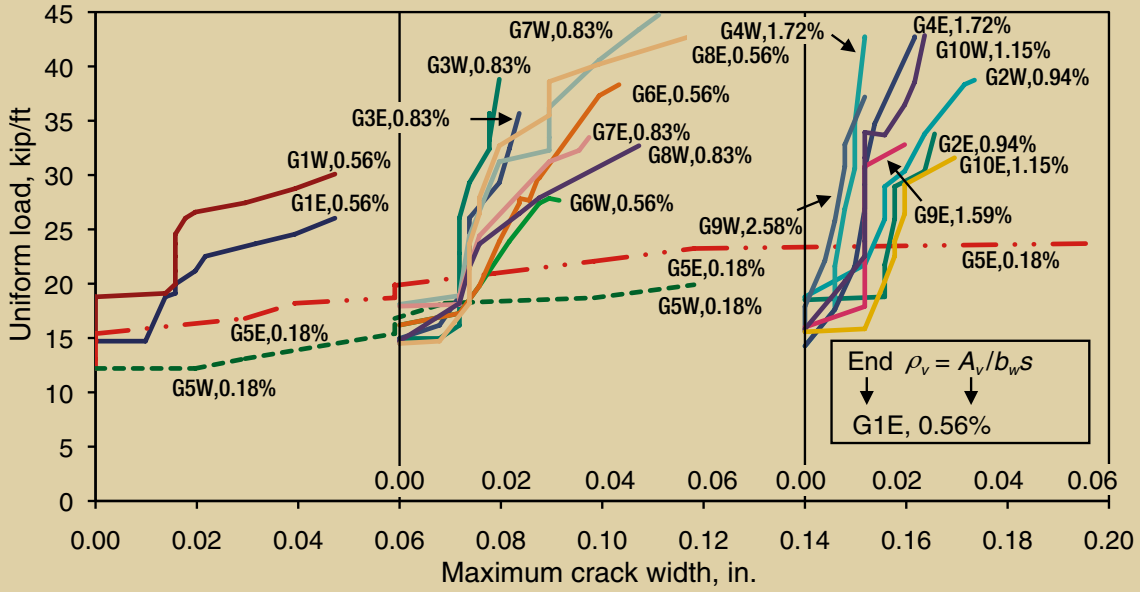

Figure 4. This graph shows the maximum widths of the web-shear cracks. Note: A_v = area of stirrups; b_w = web width; s = stirrup spacing; ρ_v = shear reinforcement ratio. 1 in. = 25.4 mm; 1 kip/ft = 14.6 kN/m.

Figure 3 shows the selected flexure-shear crack for G3E designated by the distance from the center of the support to the location of the flexure-shear crack L_{FS}. **Table 4** lists the position, angle, distributed load at cracking, moment, and shear forces of the selected flexure-shear crack. The measured angles for flexure-shear cracking ranged from 30.2 deg to 60.8 deg. The occurrence of steep shear cracks may be of concern if the member is limited by its shear capacity in this region because fewer stirrups would be carrying the load than calculated by either the AASHTO standard or LRFD specifications.

Table 4 also compares the flexure-shear cracking loads calculated by the AASHTO standard specifications to the measured values. The mean ratio of the test shear force V_{test} to the predicted shear cracking strength V_{ci} was 0.88 with a *COV* of 0.11. Therefore, the AASHTO standard specifications expression was not conservative for most of the test results. The second-to-last column of Table 4 gives the ratio of the moment at the location of the selected flexure-shear crack M to the calculated cracking moment M_{cr}. The mean ratio was 1.02 with a *COV* of 0.13. Because the flexure-shear crack typically formed as the extension of a flexural crack, the flexural cracking strength was also well predicted using a cracking stress of $6\sqrt{f_c'}$. This result also implied that the overestimation of the first term in Eq. (8) resulted in the unconservative prediction of the V_{ci} expression of the AASHTO standard specifications.

Flexural cracking

To assess when flexural cracking occurred, a displacement transducer was used to measure the change in distance over a 48-in.-long (1200 mm) section along the bottom bulb at midspan. **Table 5** compares measured and computed flexural-cracking loads.

Both the AASHTO standard specifications and the AASHTO LRFD specifications calculate the modulus of rupture f_r as $7.5\sqrt{f_c'}$ to compute the cracking moment. Table 5 also lists the predicted cracking moment and the predicted horizontal strain increase for calculations using the AASHTO standard specifications.

The predictions were based on the prestressing strains measured before testing and took into account the strain changes in the strands due to external loading. The average ratio of the measured to calculated cracking strain was 0.73 with a *COV* of 0.12, and the average ratio of the measured to calculated cracking moment was 0.88 with a *COV* of 0.06. The comparison showed that the cracking moment prediction would be a better fit if the modulus of rupture f_r was less than $7.5\sqrt{f_c'}$.

Crack widths

A crack comparator gauge was used to measure the crack widths at each load. **Figures 4** and **5** present the growth of the web-shear cracks and flexure-shear cracks with loading and also list the amount of shear reinforcement ρ_v at

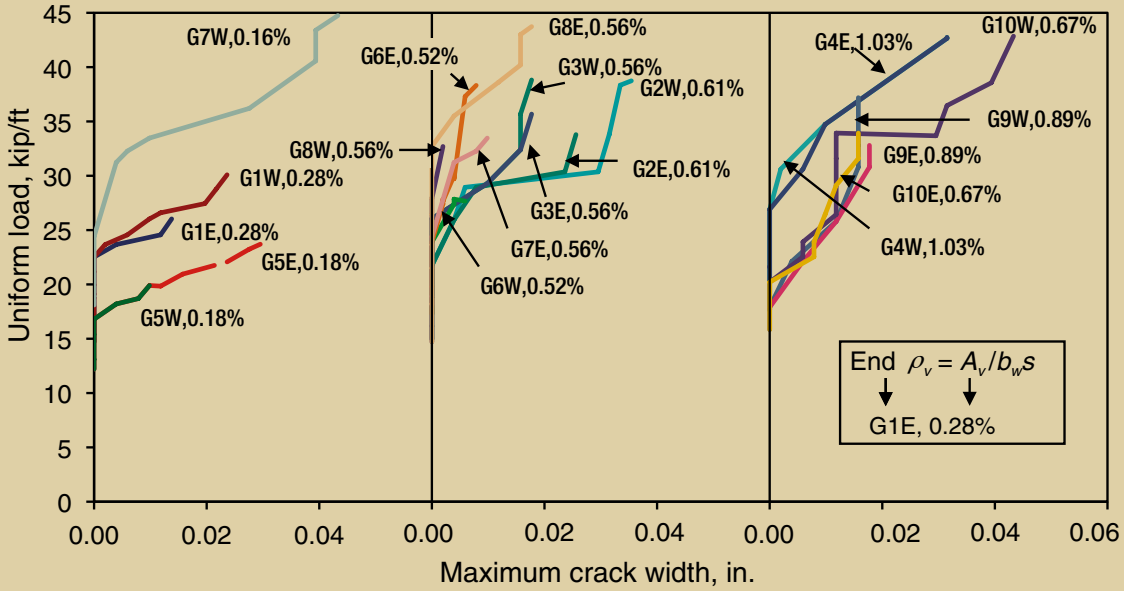

Figure 5. This graph shows the maximum widths of the flexure-shear cracks. Note: A_v = area of stirrups; b_w = web width; s = stirrup spacing; ρ_v = shear reinforcement ratio. 1 in. = 25.4 mm; 1 kip/ft = 14.6 kN/m.

each end. Once web-shear cracking occurred, the maximum crack width reached between 0.012 in. (0.3 mm) and 0.02 in. (0.5 mm). Figures 4 and 5 suggest that the maximum crack width increased linearly with loading and that the slope of this linear relationship depended on the level of shear reinforcement ratio ρ_v. Ends with low values of ρ_v were associated with greater maximum crack-width values. Equation (9) captures this observation.

$$w_{max} = \frac{v - v_{cr}}{k_w \rho_v} \tag{9}$$

where

w_{max} = maximum crack width

v = shear stress at a section

$$= \frac{V}{b_w d}$$

v_{cr} = shear stress under cracking load

k_w = constant coefficient for growth in crack width

Based on a linear regression analysis of the test data, k_w is 3200 ksi/in. (870 MPa/mm).

Figure 6 plots the measured maximum flexural cracks, where M_{cr} was calculated using a tensile fiber cracking stress of $7.5\sqrt{f'_c}$. As discussed previously, flexural cracking occurred a little earlier than predicted, as apparent from the initial M/M_{cr} values in Fig. 6. The plots show that after flexural cracking occurred, the maximum crack width increased linearly with increasing external moment.

Conclusion

A crack-recording method was developed and used to create complete and accurate crack maps for shear tests on large, simply supported prestressed concrete bulb-tee girders. This paper presented the measured cracking loads, angles, spacing, and widths from those tests. The test results were used to evaluate the performance of current methods for predictions in all aspects of cracking and as the basis for new relationships. The following conclusions were made from this examination:

- Mohr's circle of stress provides good predictions of the angle of web-shear crack. The average value was typically a little steeper than the angle of diagonal compression calculated by AASHTO LRFD specifications, suggesting that additional shear stress on the crack face is necessary to support the use of a flatter angle of diagonal compression.

- The angle of potentially critical flexure-shear cracks can be more than 60 deg, which suggests that the contribution of shear reinforcement by most codes of practice is likely to be overestimated in these regions.

- AASHTO standard specifications provide a reasonably accurate and somewhat conservative estimate of the web-shear cracking load V_{cw} but marginally

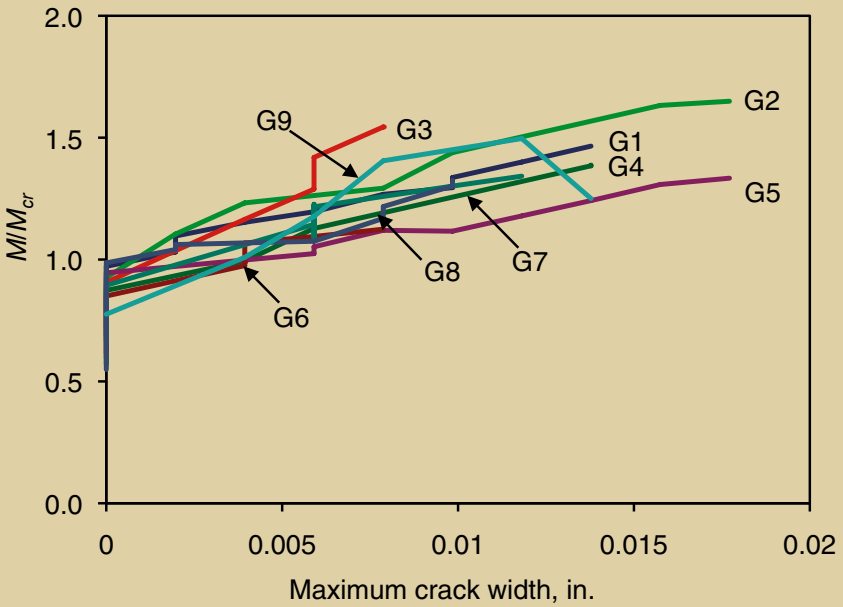

Figure 6. This graph shows the maximum widths of flexure cracks. Note: *M* = moment at the location of the selected flexure-shear crack; *Mcr* = moment causing flexural cracking at section. 1 in. = 25.4 mm.

overestimate the flexure-shear cracking loads V_{ci}. The flexural cracking loads can be predicted with reasonable accuracy by M_{cr} when the modulus of rupture f_r is calculated as $6\sqrt{f_c'}$, rather than $7.5\sqrt{f_c'}$, as suggested by AASHTO standard specifications.

- The spacing of shear cracks in the web was half the value predicted using the CEB-FIP expression for crack spacing. Equation (5), an empirical equation, was proposed based on a regression analysis of test data.
- There is a linear relationship between the maximum crack width and the external test load.

Acknowledgments

The National Academy of Science's National Cooperative Highway Research Program (NCHRP) sponsored the experimental research described in this paper as Project 12-56, *Application of the LRFD Bridge Design Specifications to High-Strength Structural Concrete: Shear Provisions.* PCI provided additional support for this research. The fabrication of the girders involved the use of high-strength concrete and heavy levels of prestressing. Wiss, Janney, Elstner Inc. developed the concrete mixture design, and Prestressed Engineering Corp. fabricated the girders at discount prices. The authors particularly acknowledge their principal co-researchers on this project, Neil Hawkins and Tom Nagle. The authors also appreciate the contributions of NCHRP program manager David Beal, the panel members for NCHRP Project 12-56, and their fellow investigators on this project, Henry Russell, Gary Klein, and Neil Anderson.

Additional acknowledgments go to Tim Prunkard and Greg Banas and their staff in the Newmark Laboratory at the University of Illinois, which handled the setup of the components for testing and managed the testing operations.

References

1. American Concrete Institute (ACI)–American Society of Civil Engineers (ASCE) Committee 426. 1973. Shear Strength of Reinforced Concrete Members. *Journal of the Structural Division*, *ASCE*, V. 99, No. ST6 (June): pp. 1091–1188.

2. Krefeld, W. J., and C. W. Thurston. 1966. Studies of the Shear and Diagonal Tension Strength of Simply Supported Reinforced Concrete Beams. *Journal of the American Concrete Institute*, V. 63, No. 4 (April–May): pp. 451–476.

3. Kim, W., and R. N. White. 1991. Initiation of Shear Cracking in Reinforced Concrete Beam with No Web Reinforcement. *ACI Structural Journal*, V. 88, No. 3 (May–June): pp. 301–308.

4. Kim, W., and R. N. White. 1999. Shear-Critical Cracking in Slender Reinforced Concrete Beams. *ACI Structural Journal*, V. 96, No. 5 (September–October): pp. 757–765.

5. Reineck, K. H. 1995. Shear Design Based on Truss Models with Crack-Friction. In *Ultimate Limit State Models*, Euro-International Concrete Committee

(CEB) Task Group 2.3, pp. 137–157. CEB-Bulletin 223. Lausanne, Switzerland: .

6. Hawkins, Neil M., Daniel A. Kuchma, Robert F. Mast, M. Lee Marsh, and Karl-Heinz Reineck. 2005. *Simplified Shear Design of Structural Concrete Members.* National Cooperative Highway Research Program (NCHRP) report 549. Washington, DC: Transportation Research Board (TRB).

7. Yamada, T., and T. Krauthammer. 1997. Crack Angle and Strain Compatibility for Shear Resistance in Reinforced Concrete Panel Structures. *ACI Structural Journal*, V. 94, No. 3, (May–June): pp. 239–247.

8. Hsu, T. T. C. 1998. Stresses and Crack Angles in Concrete Membrane Elements. *Journal of Structural Engineering*, V. 124, No. 12 (December): pp. 1476–1484.

9. Benning, W., S. Gortz, and R. Schwermann. 2000. Photogrammetriegestutzte Deformationsanalyse an Stahl- und Spannbetonbauteilen. [In German.] *Allgemeine Vermessungsnachrichten*, V. 107, No. 10 (October): pp. 346–352.

10. Hegger, J., A. Sherif, and S. Gortz. 2004. Investigation of Pre- and Postcracking Shear Behavior of Prestressed Concrete Beams Using Innovative Measuring Techniques. *ACI Structural Journal*, V. 101, No. 2 (March–April): pp. 183–192.

11. ACI 318. 2005. *Building Code Requirements for Structural Concrete (ACI 318-05) and Commentary (ACI 318R-05)*. Farmington Hills, MI: ACI.

12. Gergely, P., and L. A. Lutz. 1968. Maximum Crack Width in Reinforced Concrete Flexural Members. In *Causes, Mechanism, and Control of Cracking in Concrete*, pp. 87–117. SP-20. Detroit, MI: ACI.

13. CEB–International Federation for Prestressing (FIP). 1978. *Model Code for Concrete Structures: CEB-FIP International Recommendations*. 3rd ed. Paris, France: CEB.

14. Desayi, P. 1976. Determination of Maximum Crack Width in Reinforced Concrete Member. *Journal of the American Concrete Institute*, V. 73, No. 8 (August): pp. 473–477.

15. Oh, B. H., and Y. J. Kang. 1987. New Formulas for Maximum Crack Width and Crack Spacing in Reinforced Concrete Flexural Members. *ACI Structural Journal*, V. 84, No. 10 (March–April): pp. 103–112.

16. Frosh, R. J. 1999. Another Look at Cracking and Crack Control in Reinforced Concrete. *ACI Structural Journal*, V. 96, No. 3 (May–June): pp. 437–442.

17. Hawkins, Neil M., and Daniel A. Kuchma. 2007. *Application of the LRFD Bridge Design Specifications to High-Strength Structural Concrete: Shear Provisions.* NCHRP report 579. Washington, DC: TRB.

18. ASTM A615. 2008. *Standard Specification for Deformed and Plain Carbon-Steel Bars for Concrete Reinforcement*. ASTM International: West Conshohocken, PA.

19. Russ, J. C. 1992. *The Image Processing Handbook*. Boca Raton, FL: CRC Press.

20. Tsai, R. Y. 1987. A Versatile Camera Calibration Technique for High-Accuracy 3D Machine Vision Metrology Using Off-the-Shelf TV Cameras and Lenses. *IEEE Journal of Robotics and Automation*, V. RA-3, No. 4 (July–August): 323–344.

21. Mikhail, E. M., J. S. Bethel., and J. C. McGlone. 2001. *Introduction to Modern Photogrammetry*. New York, NY: Wiley.

22. Vecchio, F. J., and M. P. Collins. 1986. The Modified Compression Field Theory for Reinforced Concrete Elements Subjected to Shear. *Journal of the American Concrete Institute,* V. 83, No. 2 (March–April): pp. 219–231.

23. ACI Committee 408. 1966. Bond Stress—The State of the Art. *Journal of the American Concrete Institute*, V. 63, No. 11 (November): pp. 1161–1190.

24. American Association of State Highway and Transportation Officials (AASHTO). 2002. *Standard Specifications for Highway Bridges*. 17th ed. Washington, DC: AASHTO.

25. AASHTO. 2004. *AASHTO LRFD Bridge Design Specifications*. 3rd ed. Washington, DC: AASHTO.

Notation

A_v = area of stirrups across a crack

b_w = web width

c = concrete cover

c_1 = constant coefficient for crack spacing

c_2 = constant coefficient for crack spacing

c_3 = constant coefficient for crack spacing

COV = coefficient of variation

d = distance from extreme compression fiber to centroid of longitudinal tension reinforcement

d_b = bar diameter

d_v = effective shear depth

f_b = bond stress

f_c' = specified compressive strength of concrete

f_{ct} = concrete tensile strength

f_d = stress due to self-weight at extreme tensile fiber of section

f_{pc} = compressive stress at centroid of composite section

f_{pe} = compressive stress in concrete due to effective prestressing forces only at extreme tensile fiber of section

f_r = modulus of rupture

f_s = mild-steel reinforcement stress

f_t = concrete tensile strength

f_y = stress and yield strength of reinforcement

h_w = crack depth

I = moment of inertia of section

k_1 = coefficient for the bond properties of the bar

k_2 = coefficient to account for the strain gradient

k_w = constant coefficient for growth in crack width

l_b = bond length

L_{FS} = distance from the center of the support to the location of the flexure-shear crack

L_{WS} = distance from the center of the support to the location of first web-shear crack

M = moment at the location of the selected flexure-shear crack

M_{cr} = moment causing flexural cracking at section

$M_{cr,STD}$ = flexural cracking moment determined by AASHTO standard specifications

$M_{cr,test}$ = measured flexural cracking moment

M_{max} = maximum moment at section due to externally applied load

s = maximum spacing between reinforcing bars

s_m = average crack spacing

s_{mv} = average crack spacing due to transverse tension

s_{mx} = average crack spacing due to longitudinal tension

S = average crack spacing of the inclined cracks

S_{CEB} = the calculated spacing using CED-FIP approach

$S_{Eq.(5)}$ = the calculated spacing using Eq. (5) proposed in this paper

S_{test} = measured spacing

S_x = average crack spacing measured in the horizontal or longitudinal (x) direction

S_y = average crack spacing measured in the vertical or transverse (y) direction

v = shear stress

v_{cr} = cracking shear stress

V_{ci} = flexure-shear cracking strength

V_{cw} = web-shear cracking strength

$V_{cw,STD}$ = computed web-shear cracking resistance using AASHTO standard specifications

V_d = shear force at section due to self-weight

V_i = shear force at section due to externally applied load

V_p = vertical component of effective prestressing force at a section

V_s = shear capacity of the reinforcement

V_{test} = measured sectional shear force

w_{max} = maximum crack width

y_t = distance from centroidal axis of gross section to extreme fiber in tension

$\Delta\varepsilon$ = strain increment

ε_{STD} = strain determined by AASHTO standard specifications

ε_{test} = measured strain

θ = crack angle

θ_{FEA} = crack angle determined by nonlinear finite-element analysis

θ_{LRFD} = crack angle determined by AASHTO LRFD specifications

θ_{Mohr} = crack angle determined by Mohr's circle of stress

θ_{test} = measured crack angle

ρ_{ef} = effective reinforcement ratio

ρ_v = shear reinforcement ratio

About the authors

Shaoyun Sun, P.E., is a bridge engineer for Parsons in Chicago, Ill., and was a researcher for the Department of Civil and Environmental Engineering at the University of Illinois at Urbana-Champaign in Urbana, Ill.

Daniel A. Kuchma is an associate professor for the Department of Civil and Environmental Engineering at the University of Illinois at Urbana-Champaign.

Kang Su Kim is an assistant professor for the School of Architecture and Architectural Engineering at the University of Seoul in Seoul, Korea.

Synopsis

The angle, spacing, and width of shear cracks, and the loads at which shear cracks form, are all informative and externally measurable data for assessing the condition of structural concrete members. Unfortunately, there is little data on crack development from experiments on full-sized prestressed concrete bridge members.

A large experimental research program was conducted on the shear behavior of 63-in.-deep and 72-in. deep (1600 mm and 1850 mm) bulb-tee girders that were simply supported and subjected to uniformly distributed loads. In this program, a crack-recording method, based on the principles of close-range digital photogrammetry, was used to create complete and accurate crack maps that tracked the development of cracking. It was observed in this research that the angle of diagonal cracking could be predicted using Mohr's circle of stress.

The research also found that the 17th edition of the American Association of State Highway and Transportation Officials' *Standard Specifications for Highway Bridges* provided a reasonably accurate but somewhat conservative estimate of the web-shear cracking load V_{cw} and a marginally overestimated value of the flexure-shear cracking load V_{ci}. The flexural cracking loads were reasonably predicted by the calculated cracking moment M_{cr} when the tensile cracking stress was taken as $6\sqrt{f_c'}$, where f_c' is the specified compressive strength of concrete. Based on test data, equations for computing the average spacing and maximum crack width of inclined cracks were proposed to overcome the deficiencies of current methods.

Keywords

Cracking pattern, cracking strength, crack spacing, high-strength concrete, flexure shear, photogrammetry, web shear.

Review policy

This paper was reviewed in accordance with the Precast/Prestressed Concrete Institute's peer-review process.

Reader comments

Please address any reader comments to *PCI Journal* editor-in-chief Emily Lorenz at elorenz@pci.org or Precast/Prestressed Concrete Institute, c/o *PCI Journal*, 209 W. Jackson Blvd., Suite 500, Chicago, IL 60606.